

# Wire-Bonding Process Monitoring Using Thermopile Temperature Sensor

Shivesh Suman, Michael Gaitan, *Senior Member, IEEE*, Yogendra Joshi, and George G. Harman, *Fellow, IEEE*

**Abstract**—This work presents an approach to separate the thermal response due to ultrasonic excitation and ball deformation through novel application of aluminum–polysilicon thermopile sensors under the bond pad. These integrated thermopile sensors measure temperature at a radial distance under the bond pad, in contrast to the previously reported average measurements over the bond pad interface or around the bond pad over a radial distance. The high sensitivity and signal-to-noise ratio (SNR) of the sensor allow direct measurements of the signal, without any amplification or filtration. Transient temperature variations at two radial locations were obtained using two versions of thermopile sensor designs. The sensor response was interpreted using representative finite-element thermal modeling for the process. Results from modeling reveal that the thermal response is a strong function of radial location. These results also reveal that the thermal response due to interfacial heating is significantly higher under the bond pad, as compared to that around the bond pad. This is in agreement with the experimental observations. Critical points on the temperature variation curve were identified. These points can be used to correlate the sensor response to shear test data. Once the sensor response is calibrated, it can be used to monitor the bonding process. Measurements were performed at substrate temperatures of 150 °C and 200 °C, along with the microwelds characterization at the bonding interface. The comparison of the thermal response and the microwelds at the two substrate temperatures revealed that in order to correlate the sensor response to shear test data, the response must be obtained at the intended temperature of operation since the microwelds at two temperatures may be quite different, even though thermal responses may look similar.

**Index Terms**—CMOS compatible microelectromechanical system (MEMS), *in situ* process monitoring, Seebeck effect, thermopile temperature sensor, thermosonic ball bonding.

## I. INTRODUCTION

THE temperature at the bonding interface and its variation during the bonding process is both of fundamental and applied significance. The rate of heat generated during the bonding process, and the maximum temperature that the interface reaches during the process have been sources of debate in the past [1], [2]. Accurate measurement of temperature is essential for verifying and further developing the analytical models reported in the past [3], [4].

Manuscript received September 8, 2003; revised August 23, 2004. This work was supported by the National Institute of Standards and Technology Office of Microelectronic Programs. The work of Y. Joshi and S. Suman was also supported by the National Institute of Standards and Technology Grant 60NANB2D0095.

S. Suman and Y. Joshi are with the Georgia Institute of Technology, Atlanta, GA 30318 USA (e-mail: gtg697d@acme.gatech.edu).

M. Gaitan and G. G. Harman are with the Semiconductor Electronics Division, National Institute of Standards and Technology, Gaithersburg, MD 20899 USA.

Digital Object Identifier 10.1109/TADVP.2005.848696

Temperature measurements may also be utilized for process monitoring and bondability analysis. In the present study, direct measurements of thermal response at two radial locations under the bond pad were made using aluminum–polysilicon thermopile sensors. The measurements were accompanied with representative thermal modeling for the bonding process. An approach to separate the thermal response due to ball deformation and that due to ultrasonic (US) energy was suggested, and can be applied to optimize the bonding process, or monitor it in real-time. The present work, therefore, is a step toward better bonding process control using transient temperature measurements. Some of the approaches on transient temperature measurements reported in the literature are reviewed below followed by further details on the present approach.

Schneuwly *et al.* [5] reported temperature measurements as a tool for bondability analysis. Temperature was measured using gold–nickel thermoelectric junction. The junction was realized inside the inner chamfer of the modified capillary by introducing a nickel wire, which remained in contact with the ball during the bonding operation. The thermal response, thus, obtained represented temperature variation at the ball and capillary interface. The study concluded that good bonds were accompanied with a greater temperature rise and this could be used to compare the bondability on different bond pads. Another study by Falk [6] reported temperature measurements during wedge bonding. The bonding interface itself was used as the thermocouple junction. A greater bond deformation was found to be accompanied with higher temperature rise. Both these studies effectively measured the average temperature over the bonding interface. In addition, the measurement technique used in both the studies pose constraints on the wire material.

An alternative approach, which neither requires modification of the capillary nor poses any constraints on the ball material, is to use CMOS-compatible temperature sensors embedded in the chip. Mayer *et al.* [7] used serpentine resistive sensors for temperature measurements during the wire bonding process. The sensor spanned a radial distance around the pad, and thus, the thermal response represented average temperature over that distance. The sensitivity of this resistive sensor was limited by the low temperature coefficient of resistance of pure aluminum and, thus, the thermal response required amplification. In the packaging industry, shear strength of bonded ball is the parameter used to select the process window. The study by Mayer *et al.* [7] demonstrated that with the substrate at room temperature, the temperature rise due to the application of US energy could be used, instead of shear strength, to obtain the optimal process window. These results were obtained below normal thermosonic temperatures, so it was felt that further studies might be more indicative of industry usage.

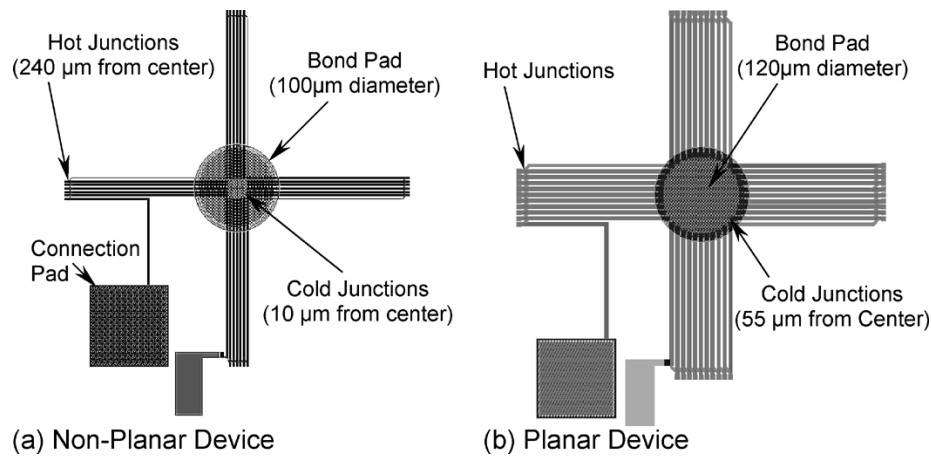


Fig. 1. Two designs of the thermopile sensor. (a) Nonplanar design: in this design the aluminum–polysilicon lines under the bond pad impart nonplanarity to the pad. (b) Planar design. In this design, the junctions are located at the periphery of the bond pad, which remains planar.

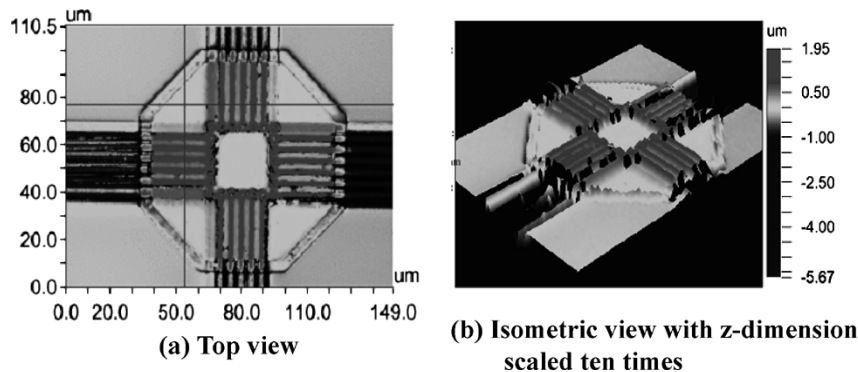


Fig. 2. Surface profile of the thermopile device. (a) Top view. (b) Isometric view. The  $z$  dimension has been exaggerated ten times to represent the nonplanarity on the pad. The bond pad has a nonplanarity of about  $1.95 \mu\text{m}$ .

The present study employs aluminum–polysilicon thermopile sensors to obtain the thermal response at a given radial location. These CMOS-compatible devices have higher sensitivity and signal-to-noise ratio compared to resistive sensors. Two variations of the sensor design were employed to measure the temperature at two different radial locations. The signals from these sensors could be acquired directly on an oscilloscope without any special amplification. Measurements were made up to a substrate temperature of  $200^\circ\text{C}$ , which is typically used in thermosonic bonding. A representative finite-element thermal model was set up to simulate the bonding process and interpret the experimentally obtained thermal response. By interpreting the measured thermal response at two radial locations, in combination with the results from simulation, a technique was devised to separate the response due to US energy and ball deformation. Measurements performed at two different substrate temperatures, accompanied with the observation of intermetallic compounds at the bonding interface, revealed that even though the thermal response may not change appreciably, the spread of the intermetallic compound over the bonding area, which governs the bond quality, might be considerably different at two substrate temperatures.

The following sections describe the layout of the sensor, the two variations of sensor design, a typical thermal response from the sensor, thermal response from two designs at two US energy input powers, results from thermal modeling, measurements and

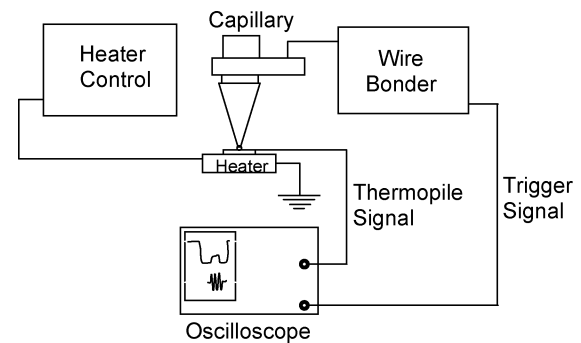


Fig. 3. Schematic of the experimental setup. The setup consists of a heater, which maintains the chip at a temperature of  $150^\circ\text{C}$  or higher. The data are acquired on a digital oscilloscope, which is triggered by the application of the US energy to the transducer.

characterization of the intermetallic compounds at two different substrate temperatures, and conclusions from the study.

## II. TEMPERATURE SENSOR

In the present study, the thermal response is obtained with an aluminum–polysilicon thermopile sensor. The thermopile is a configuration of thermocouples connected electrically in series and thermally in parallel. Fig. 1(a) and (b), respectively, show the layouts of the two sensor designs used in the present study.

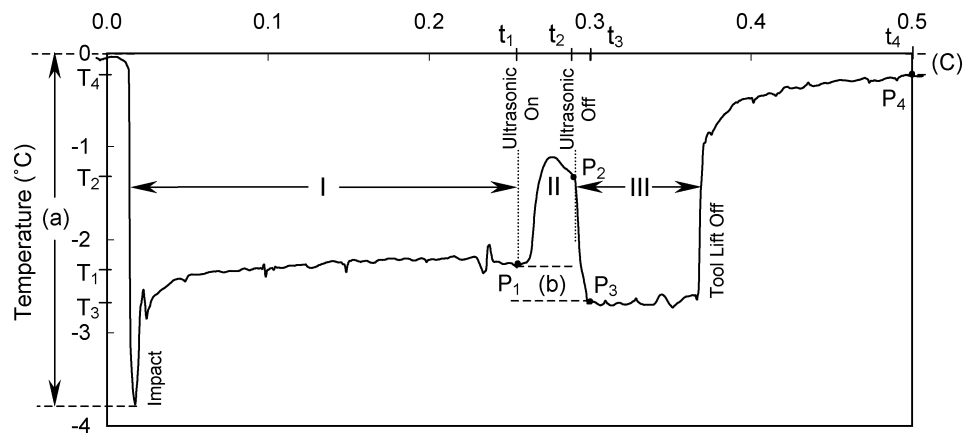


Fig. 4. Sample temperature variation measured on a planar bond pad. (a) Cooling due to ball touchdown. (b) Cooling due to ball deformation during bonding. (c) Decrease in temperature from the initial value, due to heat sinking by the deformed ball. The points P1–P4 correspond to key events in the bonding cycle.

Both designs have one set of junctions near the bonding interface and other set further away. During the bonding operation, temperature near the bonding interface varies, but remains essentially constant away from it. Thus, the thermal response from the sensor represents the temperature variation at the junctions located near the bonding interface with respect to the far-field chip temperature. Voltage across the thermopile is a net result of thermocouples connected in series to form the thermopile. Since the capillary remains at a lower temperature as compared to the chip, the junctions located near the interface are referred to as cold junctions and junctions located away as hot junctions.

The two designs shown in Fig. 1 differ in the number of thermocouples connected in series. The first design [Fig. 1(a)] consists of 24 thermocouples with the cold junctions located under the bond pad along the edge of a square of side  $40\ \mu\text{m}$ . The second design [Fig. 1(b)] consists of 40 thermocouples connected in series, with the junctions placed along a circle of diameter  $110\ \mu\text{m}$ . In the first design, the junctions remain under the ball footprint during the bonding operation. The bond pad is, thus, nonplanar due to presence of thermocouple lines under it. This is illustrated in Fig. 2, which shows the surface profile of this sensor. In the second design, the junctions are placed such that they remain around the periphery of the bonded ball, resulting in a planar bond pad. Average thermal response for both the designs is obtained by dividing the measured thermal response by the number of thermocouples connected in series.

The average response is proportional to the temperature difference between the junctions close to the bonding interface and the junctions further away, with the constant of proportionality being the Seebeck coefficient of the aluminum–polysilicon thermocouple junction. The experimental setup and a typical average thermal response are discussed next.

### III. EXPERIMENTAL SETUP

Fig. 3 shows the schematic of the experimental setup. The setup consists of a manual ball bonder (K&S 4024),<sup>1</sup> a heater,

<sup>1</sup>Commercial equipment and software referred to in this paper are identified for informational purposes only, and does not imply recommendation of or endorsement by the National Institute of Standards and Technology, nor does it imply that the products so identified are necessarily the best available for the purpose.

which maintains the mounting stage and substrate at a constant temperature, and a digital oscilloscope on which data is acquired. The oscilloscope was triggered on application of US energy to the transducer. Transient temperature variation during formation of the ball bond for the period between capillary touchdown and liftoff was logged on the oscilloscope. Fig. 4 shows a sample thermal response thus obtained using the planar device. This response is a measure of temperature variation at the junctions near the bonding interface (cold junctions), with respect to the chip and is interpreted in three stages. Stage I consists of cooling of the bond pad by the capillary touchdown followed by a partial recovery of temperature. Initially, the entire chip is at a constant temperature, and thus, the output voltage of the thermopile is zero. Temperature of the ball-capillary assembly is close to that of the ambient, thus as the capillary touches down on the bond pad, the temperature at the thermocouple junctions drops rapidly, governed by the thermal contact of two semi-infinite bodies at unequal temperatures. The steep drop is followed by a partial recovery in temperature due to flow of heat from the heated chip to the capillary. Stage II is the thermal response due to application of US energy. The rise and drop in temperature correspond respectively to the switching-on and switching-off of the US energy excitation to the capillary. This stage is of special interest for bond monitoring, as the bonding (welding) at the interface is realized in this stage. The response in this stage is a superposition of the responses due to US energy excitation and ball deformation. Thermal response between the end of the US energy excitation and the tool lift off constitutes stage III, during which the capillary rests on the bond pad without any US excitation. The temperature remains constant until the tool lifts off. After the tool liftoff, temperature recovers to a constant value, below the initial chip temperature due to the heat sinking by the ball, which is now bonded to the pad. Mayer *et al.*, [7] reported similar thermal response using resistive sensors.

The main objective of measuring the thermal response is to extract information about the US energy and the ball deformation. To facilitate this, four critical points are defined on the response as described next.

Fig. 4 shows the four critical points P<sub>1</sub>, P<sub>2</sub>, P<sub>3</sub>, and P<sub>4</sub> on the sample thermal response discussed above. Times at these

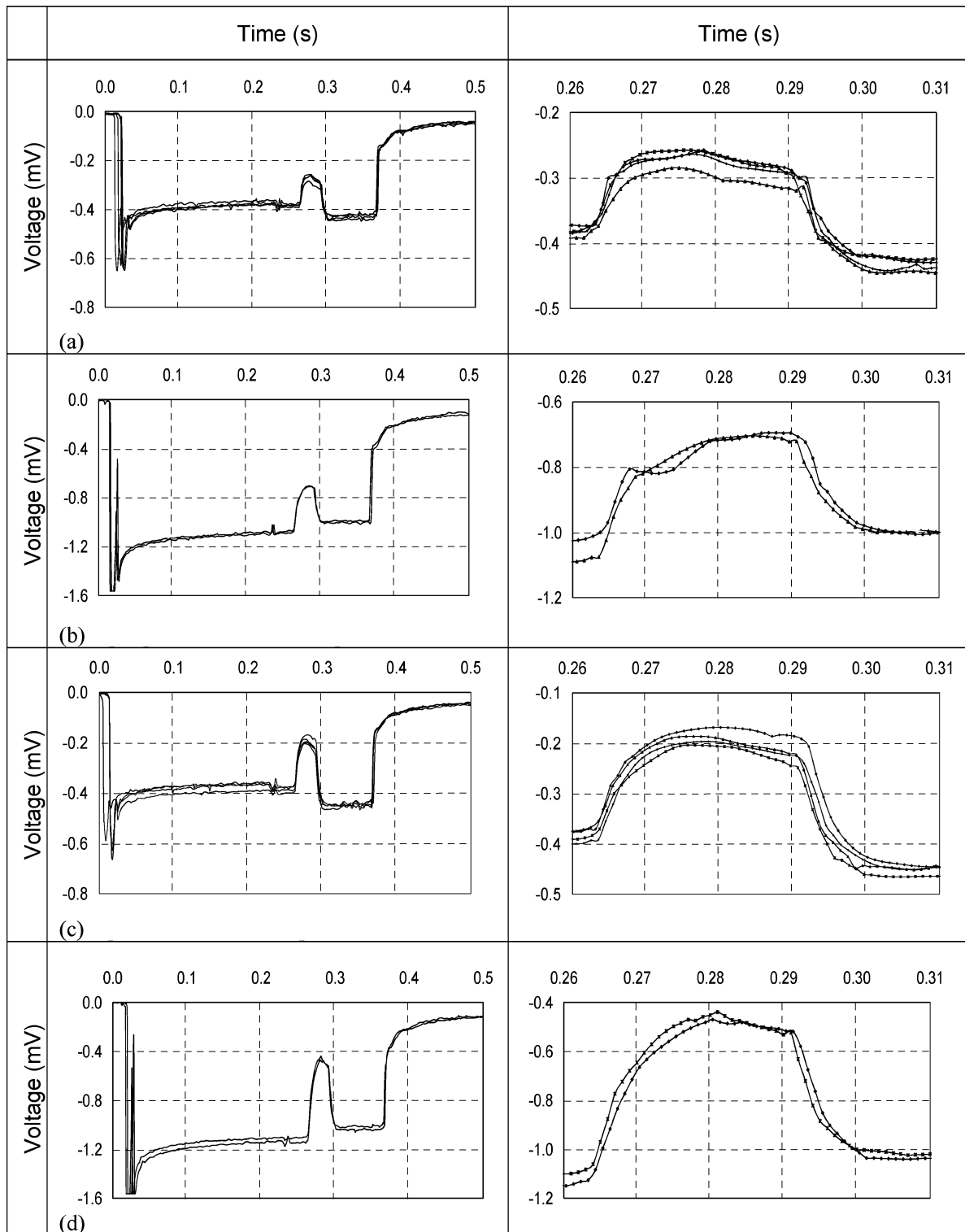


Fig. 5. Comparison of the thermal response on the planar and nonplanar bond pads. Plot on the left shows the full response of the sensor and corresponding plot on the right shows the response during the application of US energy. The response on nonplanar pads is higher than that on the planar pads because the thermocouple junctions under the nonplanar pads are closer to the bonding interface. (a) Input power = 0.22 W, planar device. (b) Input power = 0.22 W, nonplanar device. (c) Input power = 0.35 W, planar device. (d) Input power = 0.35 W, nonplanar device.

instants are denoted by  $t_1$ ,  $t_2$ ,  $t_3$ , and  $t_4$ , and the respective temperatures are denoted by  $T_1$ ,  $T_2$ ,  $T_3$ , and  $T_4$ .  $T_1$  represents the temperature just before the application of US energy.  $T_2$  is the temperature right after the US energy switches off.  $T_3$  corresponds to the steady state temperature at the end of US

excitation with the capillary still contacting the welded ball.  $T_4$  represents the temperature after the tool liftoff, with the ball bonded to the pad. The next section compares thermal responses at two radial locations, obtained using two device designs.

#### IV. EXPERIMENTAL RESULTS

Two device designs shown in Fig. 1 measure temperature under the ball footprint (at radial location  $10\ \mu\text{m}$ ) and outside (at radial location  $55\ \mu\text{m}$ ) the ball footprint. These thermopiles are single use devices, as each measurement is made by forming a bond on a new pad. To establish repeatability of the measurement, bonds were made on multiple bond pads, with identical bonder settings, and resulting responses were plotted on the same set of axes. Fig. 5 displays a set of such thermal responses in two columns. Thermal responses are average voltage readout from individual thermocouple elements and they can be converted to temperature difference between hot and cold junction using the measured Seebeck coefficient ( $130\ \mu\text{V}/^\circ\text{C}$ ) of aluminum–polysilicon thermoelectric junction [9]. Curves in the left column present full thermal response, and corresponding curves on the right represent the response during stage II, when the US energy is applied. There are two important differences between the responses at the two radial locations: 1) the temperature rise, due to US energy, under the bond pad (nonplanar device) is comparatively higher than that around the bond pad (planar device), and 2) the temperature under the bond pad (nonplanar device) increases at the end of the bonding operation than before, whereas an opposite trend is observed for temperature around the bond pad (planar device). These differences are explained with the help of modeling in the next section.

#### V. COMPUTATIONAL MODELING OF TEMPERATURE RESPONSE DURING BALL BONDING

The thermal modeling performed as part of this study had two objectives: 1) to compute the transient thermal response as a function of radial distance and study the effect of sensor placement on its response and 2) to devise an approach to monitor US power as well as ball deformation by separately simulating the response due to the two physical effects: heating at the interface due to US energy and change in steady-state temperature profile due to ball deformation. This section describes how these two objectives were met with the help of a simple thermal model.

The physical mechanism(s) which lead to temperature rise during application of US energy is (are) not completely understood. Several researchers [5]–[7] believe that sliding at the ball and pad interface causes the heating. Other possibilities could be that heat is a byproduct of ultrasonic softening of the ball [8] or is caused by energy released due the formation of microwelds. However, with the transient growth of microwelds at the interface, the amount of interfacial heating and its spatial distribution are not amenable to direct computation. Therefore, the effect of US energy was simulated qualitatively by applying a constant interfacial heat source at the ball and pad interface.

The steady-state response due to ball deformation was simulated by considering two ball geometries which correspond to slightly deformed (before application of ultrasonic) and fully deformed (after application of ultrasonic) geometries.

To meet the above stated objectives, an axisymmetric thermal model of the chip, ball, and capillary assembly was set up, as

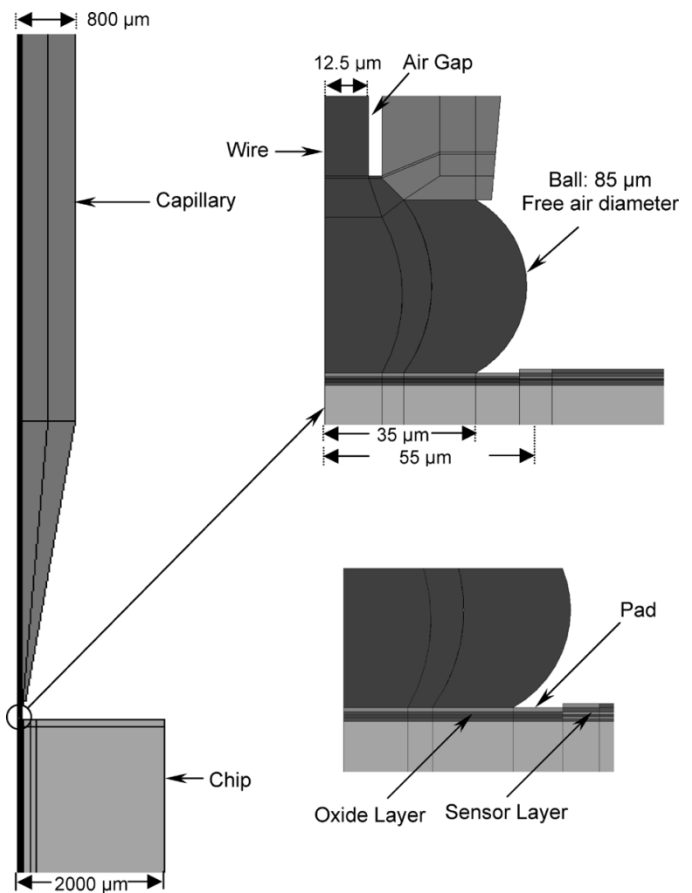


Fig. 6. Axi-symmetric computational model of the capillary and ball. The computational model consists of half the section of the capillary and the chip. The figure shows planar sensor. Nonplanar sensor was located at the radial distance of  $10\ \mu\text{m}$ .

shown in Fig. 6. Table I lists the material properties used in the model. The radial extent of the chip, as well as its height were taken sufficiently large ( $2\ \text{mm}$ ) to simulate the large thermal mass of the chip for the time duration of modeling ( $0.150\ \text{s}$ ). The capillary (414FB-0213-R35)<sup>2</sup> was modeled with its true dimensions. Owing to small thicknesses of the CMOS layers relative to the extent of computational domain, the metal and polysilicon lines were modeled as planar layers. Interfacial resistance was neglected in the model. Ball volume was taken corresponding to an initial, experimentally measured, ball diameter of  $85\ \mu\text{m}$ . Capillary and ball were prescribed room temperature ( $25\ ^\circ\text{C}$ ), and the chip was prescribed initial temperature of  $150\ ^\circ\text{C}$ . The geometry was meshed using axis-symmetric quadrilateral elements and transient temperature field was obtained using a commercial finite-element solver (Ansys).

To meet the first objective, the above described model was run with a representative heat source at the ball and pad interface, and transient temperature variation was obtained at the interface. To meet the second objective, the steady-state temperature distribution was obtained with two different ball shapes (undeformed and deformed ball geometries). The results from these simulations are discussed below.

<sup>2</sup>Kulicke & Soffa. Bonding Capillary Catalog. [www.kns.com](http://www.kns.com)

TABLE I  
MATERIAL PROPERTIES USED IN THE TRANSIENT THERMAL SIMULATION

Material	Density (Kg/m <sup>3</sup> )	Specific Heat (J/Kg-K)	Conductivity (W/m-K)
SILICON	2330	702.24	157
GOLD	19302	128.9	313.25
AIR	1.12	1005	0.027
ALUMINUM OXIDE (Capillary)	4005	1109.4	22.11
GLASS	2197.7	744.8	1.67
ALUMINUM	2700	898.7	237

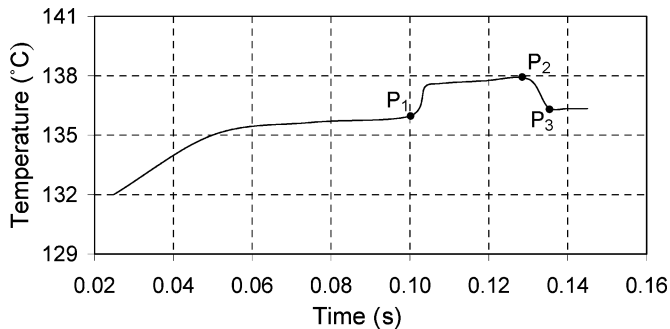


Fig. 7. Computed temperature variation at the center of the bond pad for transient thermal contact between ball and silicon chip.

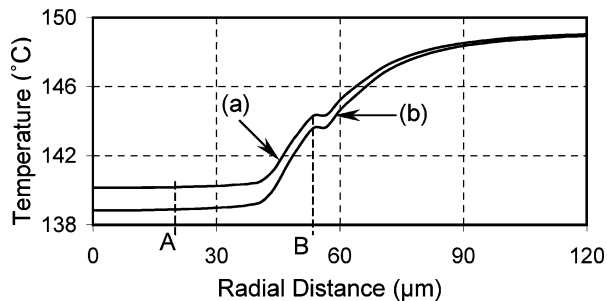


Fig. 8. Variation of temperature along the radial distance away from the center of the pad. Curve (a) represents the temperature profile before the heat source was switched off ( $P_2$ ), and curve (b) represents the temperature profile after the heat source was switched off ( $P_3$ ). "A" is the radial location of the thermoelectric junctions on the nonplanar device, and "B" is the radial location of the thermoelectric junction on the planar device.

## VI. RESPONSE DUE TO US ENERGY AS A FUNCTION OF RADIAL DISTANCE

Fig. 7 shows the temperature variation at the center of the interface as predicted by the thermal model with a uniform, planar, representative heat source. The critical points identified in Fig. 4 are indicated on the temperature variation curve obtained from simulation. This curve does not capture the thermal response due to the deformation between  $P_1$  and  $P_2$ . The drop in temperature between  $P_2$  and  $P_3$  represents the response due to switching off of the interfacial heating (US energy). The two curves in Fig. 8 show the variation of temperature, corresponding to points  $P_2$  and  $P_3$ , along the radial distance away from the center of the pad. Fig. 9 shows the difference between the two curves. It can be observed that response due to uniform heating at the bonding interface decreases rapidly with the radial distance. This is in agreement with the experimental observation of lower thermal response, due to US energy, at

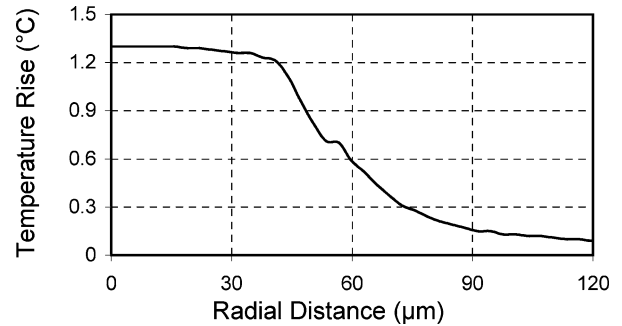


Fig. 9. Plot of temperature rise as a function of radial distance from the center of the chip, computed as the difference between the two curves (a) and (b) shown in Fig. 8. The temperature rise shows a steep decline with radial distance outside the ball footprint. Temperature rise registered by the planar devices are expected to be much lower than that registered by the nonplanar devices.

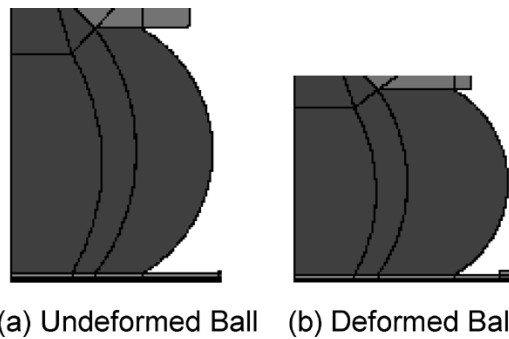


Fig. 10. Two different ball shapes. (a) Undeformed ball shape: represents the shape of the ball before the US energy is applied. (b) Deformed ball shape: represents the shape of the ball after the US energy is applied. The ball deformation is modeled as decrease in height of the ball with a simultaneous increase in the radius, with a constant total volume.

greater radial distance. The effect of ball deformation was simulated separately and is discussed next.

## VII. RESPONSE DUE TO BALL DEFORMATION

A bonded ball is significantly deformed as compared to the approximately spherical shape formed due to the electronic flame off. The deformation is realized in two steps during the bonding process. When the capillary touches down on the pad, the ball deforms slightly due to the impact. Later, it deforms significantly during the bonding process under the influence of the bonding force and the ultrasonic softening [8]. The response due to the ball deformation, which takes place in the second step, was simulated by considering two ball shapes, as representative of instants  $P_1$  and  $P_3$  in Fig. 4. These two ball shapes are shown in Fig. 10 and have equal volume. The temperatures at points  $P_1$  and  $P_3$  on the temperature variation curve are the steady state temperatures at the sensor location with undeformed and deformed ball geometry, respectively. The temperature variation as a function of radial distance, obtained from simulation, is shown in Fig. 11. It can be observed that ball deformation causes an increase in the temperature under the ball footprint and a simultaneous decrease in the temperature away from the ball footprint. The experimental results shown in Fig. 5 can be reviewed with this observation in the background. The temperature at the end of the bonding operation returned to a value higher than that before in case of

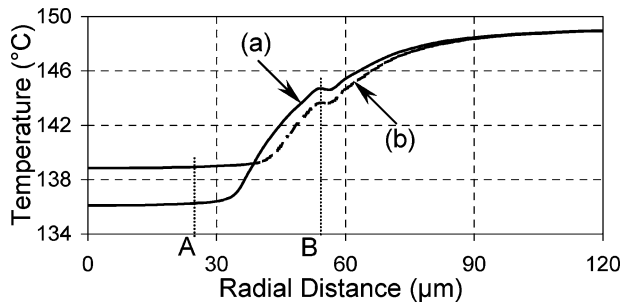


Fig. 11. Plot of temperature with the radial distance. Curve (a) represents the temperature profile with an undeformed ball, and curve (b) represents the temperature profile with a deformed ball. The deformation has an effect of homogenizing the temperature variation along the radial direction. This causes the temperature to increase under the bond pad and decrease around the bond pad.

nonplanar sensors, whereas an opposite trend was observed in case of planar sensors. Also, the temperature rise in case of the nonplanar sensors was relatively higher than the planar sensor, which is evident from the radial temperature variation shown in Fig. 8. This difference in response can be understood physically by considering the direction of the heat flow in the geometry near the bond pad. The chip is at a higher temperature than the capillary, and in the absence of an interfacial heat generation, there is a net heat flow from chip to capillary through the bonding interface. Deformation of the ball leads to an increase in the area available to this heat flow and, thus, results in an increase in the amount of heat flow from the chip to the capillary. As a result, the temperature of the capillary and the bonding interface increases, whereas due to the flow of heat from the area around the pad into the capillary, the temperature of the surrounding area decreases slightly. The net effect of the ball deformation is that of homogenizing the temperature variation along the radial direction on the substrate. In light of these results, a recommendation on where to place the cold junction, and an approach on how to process the thermal response from the sensor, is laid out. These are presented next.

### VIII. RECOMMENDATIONS ON SENSOR PLACEMENT AND POSTPROCESSING OF THE DEVICE RESPONSE

Results from modeling as well as experiment indicate that the sensitivity to ball deformation as well as US energy is significantly higher under the bond pad than that around it. However, placing the sensors at a greater radial distance allows more sensors to be placed in series and, thus, increases the sensitivity. The temperature variation presented in Fig. 11 shows that the temperature under the ball footprint is almost invariant with radial distance. Thus, it would be optimal to place the junctions such that they fall under the ball footprint, however remain at a sufficiently large radial distance, which allows placement of sufficient number of thermoelectric junctions.

Fig. 12 shows a typical response on the planar sensor. Both the US energy and ball deformation cause the temperature under the ball footprint to increase. The response due to US energy and that due to ball deformation at a particular instant can be obtained by switching the US power off at that instant. The drop in temperature after the US energy switches off represents heating

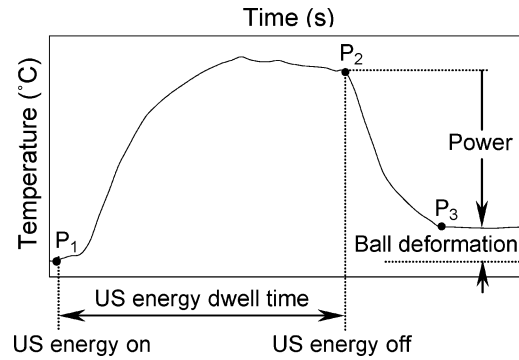


Fig. 12. Typical response due to US energy on nonplanar sensor. The response due to US power and ball deformation is shown on the response.

due to US energy at that instant. This is the difference in temperature corresponding to the points  $P_2$  and  $P_3$  and is shown in Fig. 12. The thermal response due to ball deformation is the difference between temperature before ( $P_1$ ) and after ( $P_3$ ) the application of US energy. If the effects of ball deformation and power need to be monitored at different times, the US dwell time can be varied.

To monitor the bonding process using the sensor, in real-time, the sensor response must be calibrated against the shear test data. This approach was reported in the study by Mayer *et al.* [7] in which the temperature rise due to US energy, for the bonds made at room temperature were shown to correlate with the shear strength of the bonded balls. It is important to calibrate the sensor response at substrate temperature at which the bonds are to be made, since the quality of the bonds formed may be different at two different temperatures, at identical bonding parameters. This is explained in the next section with the help of two sets of thermal responses along with the characterization of microwelds at the bonding interface.

### IX. STUDY OF THE EFFECT OF SUBSTRATE TEMPERATURE

The measurements presented in Fig. 5 were made at a substrate temperature of 150 °C. In this section, two sets of measurements at different substrate temperatures, but at an identical bonder setting, are presented. The bonds were lifted off by etching the bond pad in KOH [10]. The microwelds under the bonded balls were characterized by rotating the bonds upside down and viewing them under an optical microscope. The photomicrographs of the microwelds corresponding to the thermal response shown in Fig. 13 are shown in Fig. 14. A comparison of thermal responses and corresponding microwelds at the two temperatures reveals that even though the thermal response at two temperatures may not differ appreciably, the microwelds at the interface may be quite different. In general, it is known that at higher temperature, the microwelds are more spread out and driven deeper into the bond pad/ball [4]. Thus, the temperature variation curve must be calibrated at the temperature at which the bonds are to be made in actual process. The aluminum–polysilicon thermopiles can be used to perform direct measurements at substrate temperature of 150 °C or higher, which is commonly used for gold–aluminum thermosonic bonding.

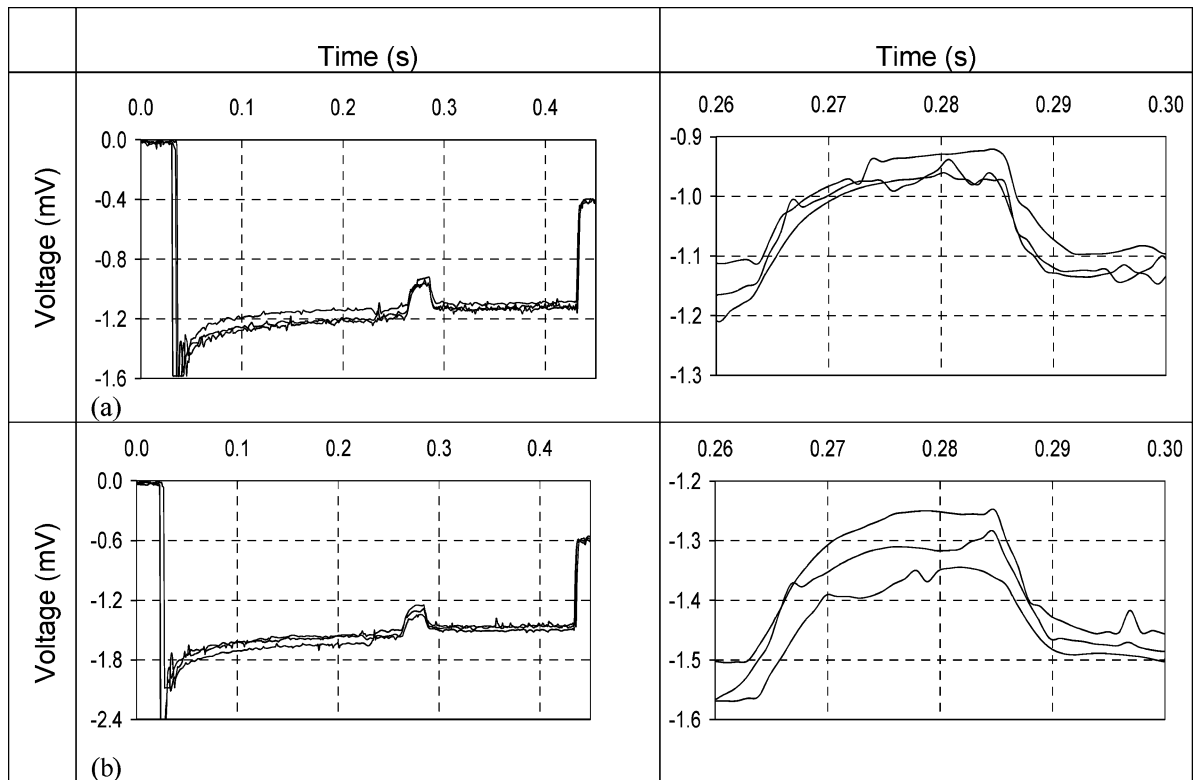


Fig. 13. Thermal response on nonplanar pads at 150 °C and 200 °C. All the bonds were made at the same power setting of 0.3 W and bonding force of 65 g. The thermal response due to the application of US energy is approximately 0.2 mV in both cases. (a) Substrate temperature: 150 °C. (b) Substrate temperature: 200 °C.



Fig. 14. Characterization of microwelds under the bonded balls corresponding to the temperature measurements presented in Fig. 13. All the bonds were made at the same power setting of 0.3 W and bonding force of 65 g. At 200 °C, the intermetallic compounds were more spread out and driven deeper (the intermetallic compound can be seen to have spread across the thickness of the bond pad) into the pad than those at 150 °C. (a) Three sample bonds made at 150 °C. (b) Three sample bonds made at 200 °C.

## X. CONCLUSION

This study demonstrated the application of CMOS compatible thermopile sensor to monitoring of the bonding process at operating temperatures for the first time. The sensor does not

require biasing. In addition, owing to its high sensitivity, the sensor allows acquisition of the thermal response without any amplification.

A technique for separating the thermal response due to ball deformation from that due to US heating was presented. The

sensor can be used to monitor both ball deformation and US power, using the recommended technique, after the sensor response is calibrated against shear test data.

The importance of calibrating the sensor response at the temperature of bonding operation was underscored by comparing the thermal response sets and the microwelds for the bonds made at substrate temperatures of 150 °C and 200 °C.

#### ACKNOWLEDGMENT

The authors would like to thank MOSIS for the fabrication of the silicon thermopile sensors.

#### REFERENCES

- [1] G. G. Harman and K. O. Leedy, "An experimental model of the microelectronic ultrasonic wire bonding mechanism," in *Proc. 10th Annu. Reliability Physics Conf.*, Las Vegas, NV, 1972, pp. 49–56.
- [2] K. C. Joshi, "The formation of ultrasonic bonds between metals," *Welding J.*, vol. 50, pp. 840–848, 1971.
- [3] H. Eigler, "A mathematical model of ultrasonic and thermosonic wire bonding," *Fachbeiträge*, vol. 9, no. 1, pp. 10–15, 1997.
- [4] A. Carrass and V. P. Jaecklin, "Analytical methods to characterize the interconnection quality of gold ball bonds," in *Proc. 2nd Eur. Conf. Electronic Packaging Technology*, vol. 173, 1996, pp. 135–139.
- [5] A. Schneuwly, P. Groning, L. Schlapbach, and G. Müller, "Bondability analysis of bond pads by thermoelectric temperature measurements," *J. Electron. Mater.*, vol. 27, no. 11, pp. 1254–1261, 1998.
- [6] J. Falk, "Thermodynamic aspect of the wire-bonding process," *Microelectron. Int.*, pp. 23–31, 1998.
- [7] M. Mayer, O. Paul, D. Bolliger, and H. Baltes, "Integrated temperature microsensors for characterization and optimization of thermosonic ball bonding process," in *Proc. Electronic Components Technology Conf.*, San Diego, CA, 1999, pp. 463–468.
- [8] H. Langenecker, "Effects of ultrasound on deformation characteristics of metals," *IEEE Trans. Sonics Ultrason.*, vol. SU-13, no. 1, pp. 1–8, Mar. 1966.
- [9] S. Suman, "Characterization of temperature variation during the wire bonding process," M.S. thesis, Dept. of Mech. Eng., Georgia Inst. Technol., Atlanta, GA, Aug. 2002.
- [10] D. T. Rooney, J. B. Dixon, K. G. Schurr, and M. R. Northrup, "Evaluation of wire bond quality by SEM analysis of ball-shape and visual inspection of intermetallic formation," in *Proc. ISHM*, 1996, pp. 432–443.



**Shivesh Suman** received the Bachelor of Technology degree in mechanical engineering from the Indian Institute of Technology, Kanpur, India, in 1999 and the M.S. degree in mechanical engineering from the Georgia Institute of Technology, Atlanta, in 2002, where he is currently pursuing the Ph.D. degree.



**Michael Gaitan** (SM'95) received the B.S., M.S.E.E., and Ph.D. degrees from the University of Maryland, College Park, in 1988, 1982, and 1980, respectively.

He is the Project Leader of the Microelectromechanical Systems (MEMS) Project, Semiconductor Electronics Division, National Institute of Standards and Technology (NIST), Gaithersburg, MD. He is developing MEMS-based test structures, test methods, and measurement standards for the MEMS and IC industries. In addition to standardization activities, he is also developing new MEMS-based measurement devices or tools that improve the accuracy of NIST calibration facilities. He has been exploring the development of CMOS MEMS-based structures such as microheating elements and passive microwave components. He is also recognized for developing the cif-MEMS process with MOSIS, one of the first MEMS foundry services in the United States.

Dr. Gaitan is a Member of Tau Beta Pi, Eta Kappa Nu, and Sigma Xi.



**Yogendra Joshi** received the Bachelor of Technology degree in mechanical engineering from the Indian Institute of Technology, Kanpur, India, in 1979, the M.S. degree in mechanical engineering from the State University of New York, Buffalo, in 1981, and the Ph.D. degree in mechanical engineering and applied mechanics, from the University of Pennsylvania, Philadelphia, in 1984.

He is a McKenney/Shiver Distinguished Professor and Associate Chair for Graduate Studies in the G. W. Woodruff School of Mechanical Engineering at

the Georgia Institute of Technology, Atlanta. He is involved in research and instruction in the area of thermal engineering associated with emerging technologies. Prior to joining the Georgia Institute of Technology in fall 2001, he held academic positions at the University of Maryland, College Park (1993–2001) and the Naval Postgraduate School (1996–1993). He is the author or coauthor of about 140 journal articles and conference papers. He has served as an academic advisor to over 30 graduate students.

Prof. Joshi was Associate Technical Editor of the American Society of Mechanical Engineers (ASME) *Journal of Electronic Packaging* from 1996 to 2001. He is an elected Fellow of the ASME and the American Association for the Advancement of Science. He was a corecipient of the 1999 ASME Curriculum Innovation Award. In 2001, he received an Inventor Recognition Award from the Semiconductor Research Corporation.



**George G. Harman** (SM'75–F'82) received the B.S. degree in industrial physics from the Virginia Polytechnic Institute and State University, Blacksburg, and the M.S. degree in physics from the University of Maryland, College Park.

He has published over 60 papers, two books on wire bonding, six book chapters, edited Kluwer books, and is the holder of four patents. He has presented numerous talks and teaches eight-hour short professional training courses for universities [University of Arizona (two per year—15 years),

IMRE (part of NUS), HKUST, and Professional Societies (IMAPS—yearly since 1983, IEEE-Components, Packaging, and Manufacturing Technology Society, DVS-(the German Welding Society), etc.]. Currently, he serves as a national and international consultant in the field of wire bonding and electronic packaging.

Mr. Harman received many awards from the IEEE, IMAPS, DVS, SME, and the National Institute of Standards and Technology (NIST). He is a Fellow Emeritus of NIST and IMAPS, and has been a Research Fellow at the University of Reading, U.K. He was the 1995 President of ISHM (IMAPS), and chaired the IEEE CPMT Fellows committee for 15 years as well as many other professional society activities. He is on the ITRS Roadmap Committee for Assembly and Packaging.